Materials Physics and Mechanics 27 (2016) 42-52 Received: March 31, 2016

MICROMECHANICS OF TWINNING AND DETWINNING PROCESSES IN NANOCRYSTALLINE AND ULTRAFINE-GRAINED METALS

I.A. Ovid'ko[1,2,3], A.G. Sheinerman[1,2,3,*], N.V. Skiba[1,2,3]

[1]Institute for Problems of Mechanical Engineering, Russian Academy of Sciences, St.Petersburg, 199178, Russia

[2]Research Laboratory for Mechanics of New Materials, Peter the Great St. Petersburg Polytechnic University, St. Petersburg, 195251, Russia

[3]Department of Mathematics and Mechanics, St. Petersburg State University, St. Petersburg, 198504, Russia

*e-mail: asheinerman@gmail.com

Abstract. We provide a brief overview of theoretical models that address twinning and detwinning processes in nanocrystalline and ultrafine-grained metals. In particular, we discuss and compare special mechanisms for formation of nanoscale deformation twins at grain boundaries (GBs) in nanocrystalline and ultrafine-grained materials. The twinning mechanisms represent (i) the successive events of partial dislocation emission from GBs; (ii) the cooperative emission of partial dislocations from GBs; and (iii) the multiplane nanoscale shear generated at GBs. In addition, we examine the detwinning mechanism in ultrafine-grained nanotwinned metals through stress-driven migration of incoherent boundaries of nanoscale twins. We demonstrate that detwinning of ultrathin twins can occur at very low stresses, while detwinning of thicker twins requires high applied stresses, and these theoretically revealed conclusions are well consistent with recent experimental data.

1. Introduction

Specific deformation mechanisms effectively operate in nanocrystalline and ultrafine-grained bulk materials, strongly influencing the outstanding mechanical properties of these solids. For instance, lattice dislocation slip in nanocrystalline and ultrafine-grained bulk shows dramatic behavioral deviations from its conventional counterpart in coarse-grained polycrystals. Also, specific GB deformation modes highly contribute to plastic flow in nanocrystalline materials with finest grains in wide temperature intervals and carry superplasticity in nanomaterials at elevated temperatures (e.g., [1]). Besides, nanoscale twin deformation effectively operates in nanomaterials with various chemical compositions and structures (e.g., [2]). In contrast to coarse-grained polycrystals where deformation twins are typically generated within grain interiors, in nanomaterials under a mechanical load, twins are often generated at GBs (e.g., [2]). In order to explain this, it was suggested that nanoscale deformation twinning occurs through successive emission of partial dislocations from GBs [2–5]. According to this explanation scheme, partial dislocations should result from the transformations of pre-existent GB dislocations located on every slip plane to form a single twin through dislocation emission from the GB. Zhu with co-workers [4, 5] suggested that multiplication of partial dislocations can occur through dislocation reactions and cross-slip processes in deformed nanomaterials. As a result of such defect transformations, partial dislocations can exist at a GB on every slip plane, in which case their successive emission events induces continuous twin growth [4, 5]. However, within this explanation, each dislocation reaction transforms a partial dislocation

into two dislocations: a full dislocation and another partial dislocation. As a corollary, the dislocation reactions in question are characterized by very large energy barriers being of the order of the full dislocation energy, which is unlikely. Within another approach briefly described earlier [6, 7], nanoscale deformation twins are generated at locally distorted GBs that contain local, deformation-distorted fragments with GB dislocations located on every slip plane and produced by preceding deformation processes. The twinning mechanisms represent (i) the successive events of partial dislocation emission from GBs; (ii) the cooperative emission of partial dislocations from GBs; and (iii) the multiplane nanoscale shear generated at GBs. The geometry of these mechanisms and the comparison of the critical stresses for their realization will be discussed in the next section.

In parallel with conventional ultrafine-grained metals, in recent years, particular attention has been devoted to ultrafine-grained metallic materials containing high-density ensembles of nanoscale twins within grains (hereinafter called nanotwinned metals), because of the outstanding combination of their superior strength and functional ductility at room temperature (see, e.g., reviews [8–11]). The specific deformation modes operating in nanotwinned metals are conventionally treated to be lattice dislocation slip hampered by twin boundaries and plastic deformation occurring through migration of coherent twin boundaries (CTBs) [8–11]. Also, recently, using transmission electron microscopy, several research groups observed detwinning of nanotwinned Cu occurring via migration of incoherent twin boundaries (ITBs) under indenter loading [12–16]. In particular, Liu et al. [14, 16] observed migration of an ITB with the length of 5.5 nm in nanotwinned Cu at ultralow indentation stress of 0.1 GPa, well below the stress needed for macroscopic yielding. Wang et al. [12], using molecular dynamics simulations, confirmed that in the case of ultrathin twins with a thickness below 2 nm, ITB migration can proceed at low shear stresses below 0.3 GPa. At the same time, the reasons for easy detwinning of thin twins in nanotwinned Cu are not yet fully understood. Therefore, in section 3 we examine a theoretical model that describes the detwinning processes in nanotwinned metals and calculates the critical parameters for the onset of detwinning in such metals.

2. Mechanisms for Formation of Nanoscale Deformation Twin at Locally Distorted Grain Boundaries in Nanomaterials

Following [7], let us examine the mechanisms for the formation of nanoscale deformation twin at locally distorted grain boundaries in nanomaterials. Within our description, nanoscale deformation twins are generated at locally distorted GBs, that is, GBs containing local fragments, rich in GB dislocations produced by preceding deformation processes. For instance, such local GB fragments can be formed due to either splitting of extrinsic lattice dislocations trapped at GBs or GB deformation processes involving slip and climb of GB dislocations. In a typical situation, the extrinsic dislocation that undergoes the splitting transformation at a GB represents a head dislocation of a pile-up configuration stopped by the GB. In this case, after the splitting of the head dislocation of the pile-up, its subsequent dislocations can reach the GB and split into new GB dislocations. Another scenario for formation of local deformation-distorted fragments of GBs is related to the formation of a GB dislocation pile-up (stopped by a triple junction of GBs) due to GB sliding (Fig. 1a). These dislocations under the applied stress climb along a GB adjacent to the triple junction (Fig. 1a). Since the rate of GB dislocation slip is much larger than that of diffusion-controlled climb of GB dislocations, the combined slip and climb of GB dislocations should result in dense, wall configurations of climbing GB dislocations that can exist on every (or almost every) slip plane (Fig. 1a).

We now discuss generation of nanoscale twins at locally deformation-distorted GBs by the following three mechanisms: (i) the cooperative emission of partial dislocations from

GBs; (ii) the successive events of partial dislocation emission from GBs; and (iii) the multiplane nanoscale shear generated at GBs.

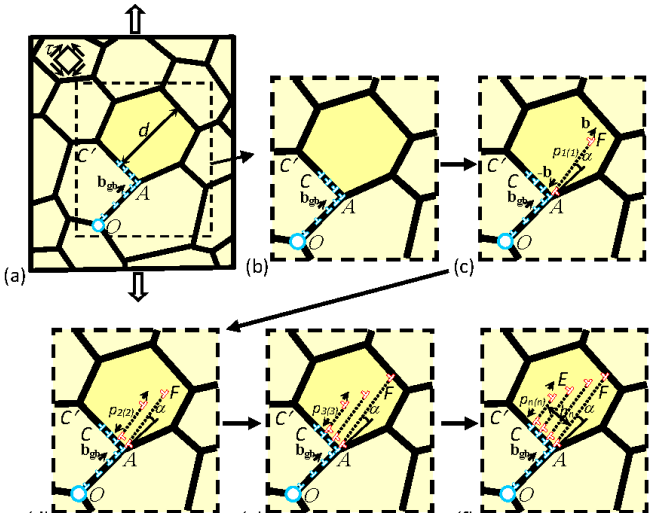

Fig. 1. Nanotwin generation occurs through successive processes of dislocation emission from a locally distorted grain boundary in a nanocrystalline specimen. (a) Nanocrystalline specimen under tensile loading (general view). Figures (b-f) highlight nanotwin generation. (b) In the initial state, nanoscale wall *AC* of climbing grain boundary dislocations (red open dislocation signs) exists at grain boundary *AC′*. (c)–(f) Successive transformations of grain boundary dislocations into sessile grain boundary dislocations and mobile partial dislocations that move in the adjacent grain interior and form nanoscale twin *ACEF*. Each such transformation is described as the formation of a dipole of partial lattice dislocations (blue open dislocation signs).

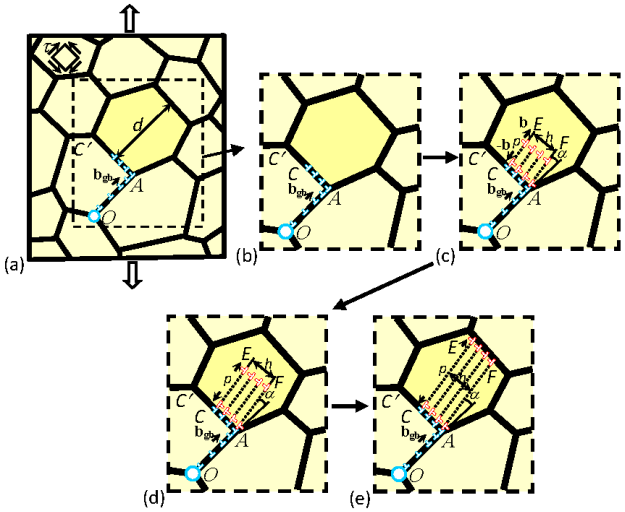

Fig. 2. Nanotwin generation occurs through cooperative dislocation emission from a locally distorted grain boundary in a nanocrystalline specimen. (a) Nanocrystalline specimen under tensile loading (general view). Figures (b)–(e) highlight nanotwin generation. (b) In the initial state, the nanoscale wall *AC* of climbing grain boundary dislocations (red open dislocation signs) exists at grain boundary *AC′*. (c)–(e) Grain boundary dislocations cooperatively transform into sessile grain boundary dislocations and mobile partial dislocations that move in the adjacent grain interior and form nanoscale twin *ACEF*. Each transformation of a grain boundary dislocation is described as the formation of a dipole of partial lattice dislocations (blue open dislocation signs).

The former two mechanisms are realized through splitting of the GB dislocations located at local deformation-distorted GB fragments into immobile GB dislocations and mobile partial dislocations (Figs. 1 and 2). The mobile dislocations move either successively (Fig. 1) or cooperatively (Fig. 2) on every slip plane within a nanoscale region where a nanoscale twin is thereby generated.

The third mechanism for nanotwin formation at a locally distorted GB is multiplane nanoscale shear (Fig. 3). Following definition in [17], a multiplane nanoscale shear represents an ideal (rigid-body) shear occurring simultaneously along several neighboring crystallographic planes within a nanoscale region – a three-dimensional region having two or three nanoscopic sizes – in a crystalline solid. The multiplane nanoscale shear within the nanoscale region is characterized by the shear magnitude s gradually growing from 0 to the Burgers vector magnitude b of a twinning partial dislocation. When s reaches value of b, a nanotwin is generated within the region in question (Fig. 3).

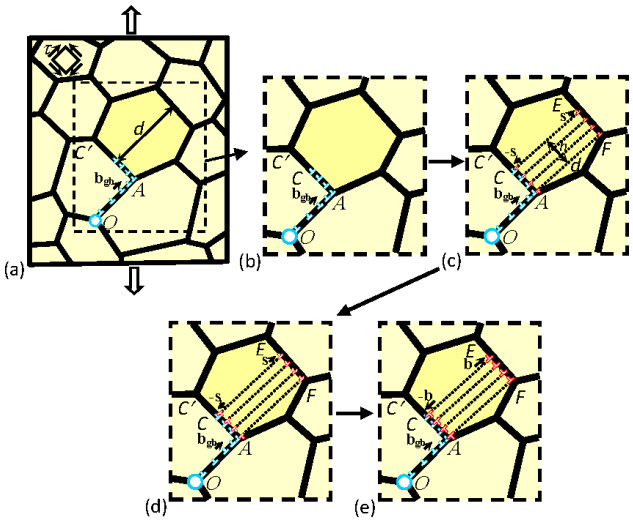

Fig. 3. Deformation nanotwinning through nanoscale multiplane shear generated at a locally distorted grain boundary in a nanocrystalline solid. (a) Nanocrystalline specimen (general view). Figures (b-e) highlight nanotwin generation. (b) In the initial state, a nanoscale wall AC of climbing grain boundary dislocations (red open dislocation signs) exists at grain boundary AC. (c) Nanoscale multiplane shear occurs which is characterized by a tiny shear magnitude *s*. Two walls of non-crystallographic dislocations (blue open dislocation signs) with tiny Burgers vectors *s* are formed at grain boundary fragments AC and EF. (d) The nanoscale shear and Burgers vector magnitude *s* gradually increases. (e) The non-crystallographic dislocations transform into twinning partial dislocations, and the nanotwin is formed.

We now consider the geometric features of nanotwin formation at locally distorted GBs in nanomaterials in the situation where local GB fragments with extra GB dislocations are formed due to both GB sliding and stress-driven climb of GB dislocations. Figure 3(a,b) illustrates a nanoscale wall configuration *AC* of GB dislocations formed at GB *AC′* as a result of such GB deformation processes. With this configuration considered as initial one, within our model, a nanoscale twin oriented along slip planes {111} is generated and evolves through successive dislocation emission events as follows.

The GB dislocations of the wall configuration can successively split into immobile GB dislocations (that stay at the GB *AC′*) and Shockley partial dislocations which are emitted from the GB *AC′* and glide along neighboring slip planes {111} (Fig. 1c-f). This transformation with associated dislocation emission events can be represented as formation of

dipoles of partial dislocations characterized by Burgers vectors $\pm b$ and joined by stacking faults (Fig. 1c-f). The stacking faults formed behind the Shockley dislocations form a nanoscale twin whose thickness grows through the successive dislocation emission events (Fig. 1c-f).

The dislocation emission and slip are driven by the shear stress τ. The first partial dislocation is emitted from the triple junction *A* and moves across the grain interior towards the opposite GB (Fig. 1c) when the shear stress reaches its critical value of τ_{c1}. When the first dislocation moves in the grain interior, a stacking fault is formed behind it (Fig. 1c). The stacking fault is characterized by the specific energy (per its unit area) γ_{sf} which serves as a hampering force for the slip of the first partial dislocation. This dislocation moves over some distance $p_{1(1)}$ in the grain interior or is stopped by the opposite GB (it depends from the level of the shear stress τ) (Fig. 1c) and creates the stress fields hampering emission of a new dislocation. As a corollary, the critical stress τ_{c2} for emission of the second partial dislocation from the GB AC' is larger than that for emission of the first dislocation: $\tau_{c2} > \tau_{c1}$. Since $\tau_{c2} > \tau_{c1}$, the first dislocation at the stress level τ_{c2} can move by the distance $p_{1(2)}$ (Fig. 1d) which is larger than the distance $p_{1(1)}$ moved by this dislocation at the stress τ_{c1} (Fig. 1c). (Hereinafter $p_{k(n)}$ denotes the distance moved by the k th partial dislocation (emitted from a grain boundary) at the critical stress $\tau_{c(n)}$ needed to emit the n th partial dislocation from this grain boundary ($n \geq k$)). At the same time, the second dislocation under the critical shear stress τ_{c2} moves over some distance $p_{2(2)}$ which is typically shorter than the distance $p_{1(2)}$ moved by the first dislocation (Fig. 1d). This is because the stress field created by the first dislocation hampers the slip of the second partial dislocation.

Note that, when the second partial dislocation moves over the distance $p_{2(2)}$, a nanoscale twin nucleus of thickness δ and length $p_{2(2)}$ is generated (Fig. 1d). The twin nucleus co-exists with a segment (of the length $p_{1(2)} - p_{2(2)}$) of the stacking fault formed behind the first partial dislocation (Fig. 1d).

Let us consider further events of the successive dislocation emission from the GB (Fig. 1e,f). In general, when the n th partial dislocation is emitted and moves over the distance $p_{n(n)}$ (Fig. 1e,f), where $n > 2$, the thickness of the nanoscale twin fragment with the length $p_{n(n)}$ increases by value of δ. In other words, a twin boundary segment with the length $p_{n(n)}$ moves over the distance δ, in which case the twin becomes thicker at its fragment of the length $p_{n(n)}$ (Fig. 1d-f). As with the first and second partial dislocations (see Fig. 1c and 1d, respectively), the critical stress $\tau_{c(n)}$ for emission of the n th dislocation is larger than that ($\tau_{c(n-1)}$) for emission and slip of the $(n-1)$ th dislocation ($\tau_{c(n)} > \tau_{c(n-1)}$), for $n > 2$. Thus, here the critical stress increases with the twin thickness.

Another mechanism represents formation of nanoscale twins through the cooperative emission of partial dislocations from locally distorted GBs in nanomaterials. As with the previous mechanism (Fig. 1), the initial defect configuration in the discussed case is a nano-sized wall of GB dislocations located on every (or almost every) slip plane in vicinities of triple junctions of GBs (Fig. 2a). The GB dislocations split into immobile GB dislocations and mobile partial dislocations that cooperatively move on every slip plane within a nanoscale region where a nanotwin is thereby generated (Fig. 2). The cooperative motion of partial dislocations typically results in the formation of a nanoscale twin having a rectangular profile with short segments located at opposite GBs (Fig. 2e). Such rectangular twins terminated at

opposite GBs were experimentally observed by high-resolution electron microscopy in nanocrystalline materials (e.g., [18]).

We now consider the third mechanism for formation of nanoscale twins, namely the nanoscale multiplane shear generated at locally distorted GBs in nanomaterials (Fig. 3). As it has been noted previously, nanoscale multiplane shear is defined [17] as a multiplane ideal shear occurring within a nanoscale region, a three-dimensional region having two or three nanoscopic sizes. The nanoscale multiplane shear is characterized by the shear magnitude s (which is identical at any time moment, for all the planes where the shear occurs), sizes of the sheared region, and the number n of the planes involved in the shear process [17]. In the examined situation with the nanoscale multiplane shear generated at a locally distorted GB (Fig. 3), a deformation twin is produced under the action of a shear stress τ (being superposition of the external stress and the sum stress created by the both the pile-up and the nano-sized wall configuration of GB dislocations; see Fig. 3) through nanoscale multiplane shear or, in terms of the dislocation theory, through simultaneous nucleation of n dipoles of non-crystallographic dislocations with tiny Burgers vectors $\pm\mathbf{s}$ (Fig. 3a-e). The non-crystallographic dislocations of the dipoles are formed at opposite GB fragments, *AC* and *EF*, on adjacent {111} planes. The Burgers vectors $\pm\mathbf{s}$ of all the dislocations are the same in magnitude and grow simultaneously from zero to the Burgers vectors $\pm\mathbf{b}$ of Shockley partials during the nanotwin formation process. In doing so, since there are pre-existent GB dislocations at the GB fragment *AC*, the non-crystallographic dislocations at the GB fragment *AC* merge with these pre-existent GB dislocations. As a corollary, during the nanotwin formation process, evolution of the non-crystallographic dislocations at the GB fragment *AC* manifests itself in evolution of the GB dislocations at this fragment (Fig. 3c-e). More precisely, since the initial state of the GB dislocation structure is specified by the presence of GB dislocations at the GB fragment *AC*, on the first stage of the evolution, their Burgers vector magnitudes gradually diminish down to 0 (Fig. 3c,d). On the second stage evolution, new GB dislocations with the Burgers vectors opposite to those of initial GB dislocations appear at the GB fragment *AC*, and their Burgers vector magnitude gradually grows until some value at which the nanotwin *ACEF* is formed (Fig. 3e).

Thus, from the geometric viewpoint, the three mechanisms for nanoscale twin formation at locally deformation-distorted GBs can come into play in nanomaterials. In order to understand which mechanism tends to dominate, we have calculated and compared the critical stresses for the activation of each mechanism [7].

Let us denote the critical stresses for twin formation via the consequent dislocation emission from a GB (Fig. 1), simultaneous dislocation emission from a GB (Fig. 2) and multiplane nanoscale shear (Fig. 3) as τ_c, τ_c' and $\tilde{\tau}_c$, respectively. The dependences of the above critical stresses on twin thickness h are presented in Fig. 4 for the case of nanocrystalline Cu with a grain size of 30 nm.

Figure 4 demonstrates that the generation of ultrathin nanotwins with thickness $h<1$ nm through cooperative emission of partial dislocations from locally deformation-distorted GBs (Fig. 2) occurs at the lowest stress level $\tau_c' < \tilde{\tau}_c < \tau_c$. At the same time, in the range of h from 1 to 2 nm, the generation of nanotwins through nanoscale multiplane shear (Fig. 3) is more favorable; it occurs at the lowest stress level. For $h>2$ nm, the cooperative emission of partial dislocations from GBs (Fig. 2) in copper is the most favorable process characterized by the lowest critical stress.

Thus, the deformation twinning mechanisms are in competition. Typically, the most favorable mechanism represents the cooperative emission of partial dislocations from GBs containing local deformation-distorted fragments (Fig. 2), because it is characterized by the lowest critical stress in a wide range of the twin thickness (Fig. 4).

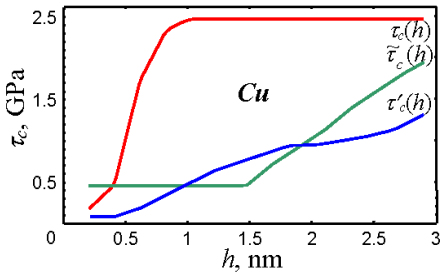

Fig. 4. Dependences of critical stresses τ_c, τ'_c and $\tilde{\tau}_c$ (specifying various micromechanisms for nanotwin generation at locally distorted grain boundaries) on nanotwin thickness h, for nanocrystalline Cu.

In parallel with deformation twinning examined in this section, stress-induced detwinning often occurs in ultrafine-grained metals. The micromechanism for this process will be examined in the next section.

3. Mechanisms for Detwinning of Nanotwinned Metals

Following [19], consider a model grain in a deformed nanotwinned metal with a face-centered cubic (fcc) lattice (Fig. 5a). Within our model, the grain is composed of growth twins divided by CTBs. We assume that an applied shear stress τ acts in the examined grain as shown in Fig. 5a. In the initial state, the model grain contains a rectangular twin CEFD bounded by grain boundary (GB) segments CD and EF and CTB CE and BF. We consider the situation where an incoherent twin boundary (ITB) AB is generated at the GB segment CD and moves along the CTBs CE and DF (Fig. 1a). In doing so, the motion of the ITB AB is accompanied by the disappearance of the CTB fragments AD and BC, thus leading to the shrinking of the twin AFEB. If the ITB approaches the GB EF, the twin AFEB completely disappears, thus promoting local detwinning in the nanotwinned solid.

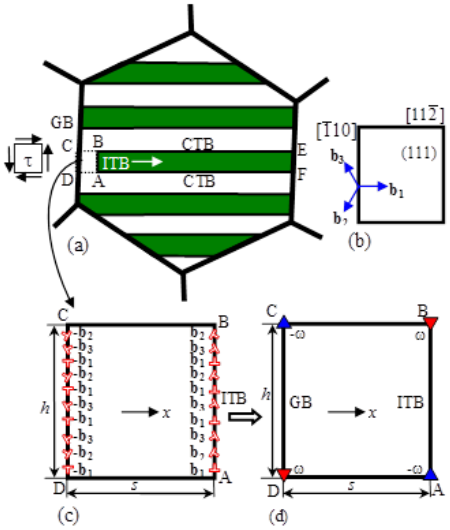

Fig. 5. Detwinning in a deformed nanotwinned metal. (a) A model grain of a nanotwinned solid under the action of an applied shear stress τ. An incoherent twin boundary (ITB) nucleates at a grain boundary and moves under the action of the applied shear stress along coherent twin boundaries (CTBs). (b) Geometry of dislocations composing the ITB. (c) A magnified region ABCD of figure (a) shows a dislocation ensemble at the ITB and an ensemble of opposite-sign dislocations at the grain boundary. (d) The dislocation structure shown in figure (c) is approximated as a quadrupole of wedge disclinations specified by the strengths $\pm\omega$.

We now consider the geometry of the formation and motion of the ITB AB. It is known that, in fcc solids, CTBs are located at {111} crystal planes, while ITBs commonly lie in {112} planes. For definiteness, we suppose that CTBs AF and BE occupy (111) crystal planes, while the ITB AB is located at a $(11\bar{2})$ crystal plane. Within our model, the formation and motion of the $(11\bar{2})$ ITB (accompanied by the shrinkage of the CTBs BE and AF) can be realized by the formation and simultaneous motion of the Shockley partial dislocations along all the (111) planes of the twin CEFD [12,13]. Each Shockley partial has the line direction $[\bar{1}10]$ and the Burgers vector $\mathbf{b}_1$, $\mathbf{b}_2$ or $\mathbf{b}_3$, where $\mathbf{b}_1 = (a/6)[11\bar{2}]$, $\mathbf{b}_2 = (a/6)[1\bar{2}1]$ and $\mathbf{b}_3 = (a/6)[\bar{2}11]$ (Fig. 5b), with a being the crystal lattice parameter. The dislocations specified by the Burgers vector $\mathbf{b}_1$ represent edge dislocations, while those with the Burgers vectors $\mathbf{b}_2$ and $\mathbf{b}_3$ are 30° mixed dislocations. The vector sum of the three Burgers vectors $\mathbf{b}_1$, $\mathbf{b}_2$ and $\mathbf{b}_3$ is zero, that is, $\mathbf{b}_1 + \mathbf{b}_2 + \mathbf{b}_3 = 0$.

Due to the conservation of the dislocation Burgers vector, each nucleating dislocation with the Burgers vector $\mathbf{b}_k$ (where $k = 1,2,3$) should leave the opposite-sign dislocation with the Burgers vector $-\mathbf{b}_k$ at the GB fragment CD (Fig. 5c). Thus, the generation and motion of the ITB CD can be realized by the formation of the dipoles of the dislocations with the Burgers vectors $\pm\mathbf{b}_k$ at each (111) plane, followed by the simultaneous motion of the dislocations with the Burgers vectors $\mathbf{b}_k$ that form the ITB AB (Fig. 5c).

For simplicity, in the following, we consider the most energetically favored ITB with the misorientations on the large-scale level being constant along the boundary. Also, since screw dislocations do not interact with the shear stress τ and, at the same time, accumulate some self-energy, the formation of the ITB with the zero screw component of the net Burgers vector is most energetically favored. For definiteness, in the following, we consider this most energetically favorable case where the screw component of the total Burgers vector of all the dislocations composing the ITB is equal to zero. In the examined case, the ITB represents a tilt boundary. In this situation, for the calculation of the self-energies that characterize the dislocation walls, the two dislocation arrays AB and CD can be approximated as a quadrupole ABCD of wedge disclinations with the strengths $\pm\omega$ (Fig. 5d). The disclination strength magnitude ω is defined as $\omega = 2\arctan(B_e/(2h))$, where B_e is the edge component of the total Burgers vector of all the dislocations composing the ITB AB and h is the length of this boundary, equal to the thickness of the examined twin AFEB (Fig. 5).

Let us calculate the critical parameters for detwinning in nanotwinned fcc metals. To do so, we calculate the projection F_x of the force $\mathbf{F}$ acting on the moving ITB (per unit boundary length in the direction normal to the plane of Figs. 5c and 5d). The force F_x can be calculated as follows [19]:

$$F_x = -\frac{dW_q}{dx} - (h/p)b\tau_p^e + \tau\omega h + 2\gamma_{CTB}, \tag{1}$$

where W_q is the self-energy of the disclination quadrupole (per unit disclination length), γ_{CTB} is the specific (per unit area) energy of the CTB, $\tau_p^e = f_1\tau_{p1} + (1-f_1)\tau_{p2}$ is the effective Peierls stress, and τ_{p1} and τ_{p2} are the Peierls stresses for the motion of the edge and mixed 30° dislocations, respectively, f_1 is the fraction of edge dislocations, $b = a/\sqrt{6}$ is the magnitude of the Burgers vectors of all the dislocations, and $p = a/\sqrt{3}$ is the distance between the adjacent (111) planes. In the isotropic approximation, the self-energy of the disclination quadrupole is given by [20]

$$W^q = \frac{D\omega^2 h^2}{2}\left[(1+t^2)\ln(1+t^2) - t^2\ln(t^2)\right], \quad (2)$$

where $t = s/h$, s is the distance between the disclination dipoles AB and CD (Fig. 5d), $D = G/[2\pi(1-\nu)]$, G is the shear modulus and ν is Poisson's ratio. Substitution of (2) to (1) and account for the relation $b/p = 1/\sqrt{2}$ yield

$$F_x = \omega h\left[-D\omega t\log(1+1/t^2) + \tau - \frac{\tau_p^e}{\sqrt{2}\omega} + \frac{2\gamma_{CTB}}{\omega h}\right]. \quad (3)$$

The minimum value $F_{\min}$ of the force F_x is reached at $t \approx 0.505$. For this value of t, we have: $t\log(1+1/t^2) \approx 0.805$. To move the ITB across the twin, the force F_x acting on this ITB should be positive at any value of t. This condition is valid, if the minimum value $F_{\min}$ of the force F_x is positive, that is,

$$-0.805D\omega + \tau - \frac{\tau_p^e}{\sqrt{2}\omega} + \frac{2\gamma_{CTB}}{\omega h} > 0. \quad (4)$$

Formula (4) can be rewritten as $\tau > \tau'$, where

$$\tau' = 0.805D\omega + \frac{\tau_p^e}{\sqrt{2}\omega} - \frac{2\gamma_{CTB}}{\omega h}. \quad (5)$$

In the following, we focus our examination on the case of nanotwinned Cu characterized by the following values of material parameters: $G = 48$ GPa, $\nu = 0.34$, and $\gamma_{CTB} = 24$ mJ/m^2 [21]. Since the exact values of the quantities τ_{p1} and τ_{p2} for Cu at room temperature are unknown, for simplicity, we put $\tau_{p1} = \tau_{p2} = 30$ MPa. The analysis of formula (5) demonstrates that, when values of h are not too small, the dependences $\tau'(\omega)$ have a minimum, whereas, for sufficiently small values of h, τ' monotonously decreases with diminishing ω. The transition from the first to the second case occurs at $h = h_c$, where $h_c = 2\sqrt{2}\gamma_{CTB}/\tau_p^e$. For nanotwinned Cu, from the latter relation we obtain: $h_c \approx 2.2$ nm. Also, formula (5) demonstrates that the formation and migration of the ITB at $h < h_c$ is favored even in the situation with $\omega \to 0$, corresponding to the zero net Burgers vector of the ITB. This result is well consistent with the experimental observation [13] of the motion of an ITB containing a dislocation array characterized by a zero net Burgers vector in nanotwinned Cu under indenter loading in the case of twin thickness being around 2 nm. Also, in the situation with $h < h_c$, the formation and migration of the ITB is favored even in the absence of the applied stress ($\tau = 0$) with the proviso that the disclination strength ω is either sufficiently small or equals zero. In the latter case (where $\omega = 0$), the driving force for the ITB migration occurs due to disappearance of the CTB fragments, that accompanies ITB motion.

One should bear in mind that the expression $h_c = 2\sqrt{2}\gamma_{CTB}/\tau_p^e$ for the critical twin thickness h_c is obtained for the "hardest" case where all the dislocations pass the maximums of the Peierls barrier for dislocation motion simultaneously. At the same time, dislocations can overcome the maximums of the Peierls stress one by one, in which case the friction force exerted by the Peierls stress on the ITB will be lower. In the latter case, the critical thickness h_c for ITB migration can be larger than $2\sqrt{2}\gamma_{CTB}/\tau_p^e$, that is, higher than 2.2 nm for Cu. This explains the experimental observation [14] of migration of an ITB with the length of 5.5 nm in nanotwinned Cu at ultra-low indentation stress of 0.1 GPa.

We now define the critical stress τ_c^d as the minimum non-negative stress (for a given twin thickness h) at which detwinning via the formation and migration of an ITB is favored at least for some values of the disclination strength ω. In other words, τ_c^d corresponds to the minimum value of τ' at $h \geq h_c$, and $\tau_c^d = 0$ at $h < h_c$. The dependence of the critical stress τ_c^d on twin thickness h for nanotwinned Cu is presented in Fig. 6. From Fig. 6 it follows that the critical stress τ_c^d quickly increases with the twin thickness h at $h > h_c$ until h reaches 5–10 nm. After that, τ_c^d only slightly increases with increasing h. Also, Fig. 6 shows that, if the twin thickness lies in the interval 5–25 nm, the critical shear stress is around 0.7–0.8 GPa. These values are higher than the typical values of the resolved shear stress during the uniaxial deformation of nanotwinned Cu, but they can be reached at some regions of nanotwinned Cu due to stress concentration or in the regions near the indenter in the case of indenter loading.

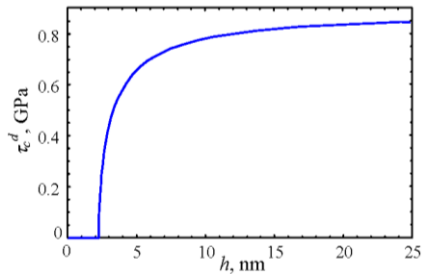

Fig. 6. Dependences of the critical shear stress τ_c^d on twin thickness h in nanotwinned Cu.

4. Conclusions

To summarize, special physical mechanisms for formation of nanoscale deformation twins at GBs can effectively operate in nanocrystalline and ultrafine-grained metals. These mechanisms involve generation of nanoscale deformation twins at locally distorted GBs that contain local, deformation-distorted fragments being rich in GB dislocations produced by preceding deformation processes. The twinning mechanisms in question represent (i) the successive events of partial dislocation emission from GBs (Fig. 1); (ii) the cooperative emission of partial dislocations from GBs (Fig. 2); and (iii) the multiplane nanoscale shear generated at GBs (Fig. 3). The calculations demonstrate that the deformation twinning mechanisms can operate in nanocrystalline and ultrafine-grained materials at rather high but realistic levels of the stress. In general, the deformation twinning mechanisms are in competition. Typically the most favorable mechanism is the cooperative emission of partial dislocations from GBs containing local deformation-distorted fragments (Fig. 2), because it is characterized by the lowest critical stress in a wide range of the twin thickness (Fig. 4).

In parallel with deformation twinning, stress-induced detwinning also occurs in nanocrystalline and ultrafine-grained metals. In particular, in nanotwinned metals detwinning can occur through stress-driven migration of ITBs (Fig. 5). It is found that the formation and migration of the incoherent boundaries of ultrathin nanotwins (characterized by $h < h_c$, where the critical twin thickness $h_c \approx 2.2$ nm for Cu) is favored even in the situation with the zero net Burgers vector of the ITB. This result is well consistent with the experimental observation [13] of the motion of an ITB containing a dislocation array characterized by a zero net Burgers vector in nanotwinned Cu under indenter loading in the case of twin thickness being around 2 nm.

Also, it is found that in the case of ultrathin twins, the detwinning process is energetically favored even in the situation where the external stress is very small. In this situation, the release of the energy of coherent twin boundaries (that disappear when the detwinning process comes into play) serves as the driving force for migration of ITBs.

Acknowledgements. *The work was supported, in part (for IAO), by the Russian Science Foundation (Research Project 14-29-00199) and St. Petersburg State University (grant 6.38.337.2015), in part (for AGS), by the Ministry of Education and Science of Russian Federation (grant MD-2893.2015.1) and the Russian Fund of Basic Research (grant 15-31-20095) and, in part (for NVS), by the Ministry of Education and Science of Russian Federation (Zadanie № 9.1964.2014/K and grant MD-9152.2016.1) and the Russian Fund of Basic Research (grant 16-32-60110).*

References

[1] C.C. Koch, I.A. Ovid'ko, S. Seal, S. Veprek, *Structural Nanocrystalline Materials: Fundamentals and Applications* (Cambridge University Press, Cambridge, 2007).
[2] Y.T. Zhu, X.Z. Liao, X.-L. Wu // *Progress in Materials Science* **57** (2012) 1.
[3] Y.T. Zhu, X.Z. Liao, X.-L. Wu // *JOM* **60** (2008) 60.
[4] Y.T. Zhu, X.-L. Wu, X.Z. Liao, J. Narayan, S.N. Mathaudhu, L.J. Kecskes // *Applied Physics Letters* 95 (2009) 031909.
[5] Y.T. Zhu, J. Narayan, J.P. Hirth, S. Mahajan, X.-L. Wu, X.Z. Liao // *Acta Materialia* **57** (2009) 3763.
[6] I.A. Ovid'ko, N.V. Skiba // *Scripta* Materialia **71** (2014) 33.
[7] I.A. Ovid'ko, N.V. Skiba // *International Journal of Plasticity* **62** (2014) 50.
[8] T. Zhu, H. Gao // *Scripta Materialia* **66** (2012) 843.
[9] X. Li, H. Gao, In: *Nano and Cell Mechanics: Fundamentals and Frontiers*, ed. by H.D Espinosa and G. Bao (Wiley, 2013), p. 129.
[10] I.J. Beyerlein, X. Zhang, A. Misra // *Annual Review of Materials Research* **44** (2014) 329.
[11] I.A. Ovid'ko, A.G. Sheinerman, In: *Nanofabrication using Nanomaterials* (One Central Press, 2016), p. 46.
[12] J. Wang, N. Li, O. Anderoglu, X. Zhang, A. Misra, J.Y. Huang, J.P. Hirth // *Acta Materialia* **58** (2010) 2270.
[13] N. Li, J. Wang, J.Y. Huang, A. Misra, X. Zhang // *Scripta Materialia* **64** (2011) 149.
[14] Y. Liu, J. Jian, Y. Chen, H. Wang, X. Zhang // *Applied Physics Letters* **104** (2014) 231910.
[15] N. Lu, K. Du, L. Lu, H. Q. Ye // *Journal of Applied Physics* **115** (2014) 024310.
[16] Y. Liu, N. Li, D. Bufford, J. H. Lee, J. Wang, H. Wang and X. Zhang // **68** (2016) 127.
[17] I.A. Ovid'ko // *Applied Physics Letters* **99** (2011) 061907.
[18] X.-L. Wu, Y.T. Zhu, E. Ma // *Applied Physics Letters* **88** (2006) 121905.
[19] I.A. Ovid'ko, A.G. Sheinerman // *Reviews on Advanced Materials Science* **43** (2015) 38.
[20] M.Yu. Gutkin, K.N. Mikaelyan, A.E. Romanov, P. Klimanek // *Physica Status Solidi A* **193** (2002) 35.
[21] R. Niu, K. Han // *Scripta Materialia* **68** (2013) 960.